Transformation in orbital reconstruction

Schreurs, R.

Publication date
2021

Chapter 10

Registration-free navigation

This Chapter is based on the following accepted manuscript:

Schreurs R., Baan F., Klop C., Dubois L., Beenen LF., Habets PEMH., Becking AG., Maal TJJ. Registration-free workflow for electromagnetic and optical navigation in orbital and craniofacial surgery. Sci Rep 2021

(Initial submission: 10-04-2020. Accepted: 13-08-2021)

ABSTRACT

The accuracy of surgical navigation is mainly dependent on the intraoperative registration procedure. Next to accuracy, essential factors to consider for the registration procedure are invasiveness, time consumption, logistical demands, user dependency, compatibility, and radiation exposure. In this study, a workflow is presented that eliminates the need for a registration procedure: registration-free navigation. In the workflow, the maxillary dental model is fused to the preoperative image data using commercially available virtual surgical planning software. A virtual dynamic reference frame on a splint is designed on the patient's fused maxillary dentition: during surgery, the splint containing the reference frame is positioned on the patient's dentition. This splint alleviates the need for any registration procedure since the reference frame's position is known from the design. The accuracy of the workflow was evaluated in a cadaver setup and compared to bone-anchored fiducial and surface-based registration. The results showed that the accuracy of the registration-free workflow was greatly dependent on the tracking technique used: the workflow was the most accurate with electromagnetic tracking but the least accurate with optical tracking. Although this method offers a time-efficient, noninvasive, radiation-free, automatic alternative for registration, clinical implementation is hampered by the unexplained differences in accuracy between the tracking techniques.

Introduction

Accurate registration is the cornerstone to acquire reliable positional information in surgical navigation.[1–9] The ideal registration method would be noninvasive, little time consuming, not logistically challenging, automatic and thus not user-dependent, usable in every patient, compatible with each tracking technique (optical and electromagnetic (EM)), not exposing the patient to additional radiation and, most of all, accurate.

Currently, several registration concepts exist in craniofacial surgery: fiducial markers, splints, or a combination of the two may be used in point-based registration.[3,5,7,10,11] Surface-based registration may be accomplished through contouring with a pointer or laser surface scanning. Next to specific drawbacks regarding the accuracy, invasiveness, and usability, each method requires user interaction. The result of the registration process will be user-dependent to some degree. Automatic image registration overcomes the user-dependency issue: intraoperative imaging is acquired with the dynamic reference frame (DRF) in place.[7,10,12] If a virtual surgical planning (VSP) is made on the preoperative image set, image fusion allows integration of the intraoperative registration scan in the VSP. While the user-dependency drawback is eliminated, issues regarding radiation exposure and extended operation time remain.

In this study, a registration-free splint-based method is proposed that eliminates user dependency and does not require the acquisition of additional intraoperative imaging. The methodology of registration-free navigation is outlined, and the accuracy is compared to bone-anchored maxillary fiducials (optical and EM) and surface-based registration (EM).

Methods

Preparations

Five dentulous cadaver heads were obtained through the body donation program from the Department of Medical Biology, Section Clinical Anatomy and Embryology of the Amsterdam University Medical Centers (location AMC), The Netherlands. The bodies were donated to science following Dutch legislation and the regulations of the medical ethical committee of the Amsterdam University Medical Centers. The experimental protocol was approved by the review committee from the Department of Medical Biology, Section Clinical Anatomy and Embryology (ref. 2018-087). All methods were performed according to the relevant guidelines and regulations. The dental status (maxilla) of the cadavers is shown in **Chapter 9** (Table 1). The fixated cadaver heads were equipped with five titanium screws (1.5 x 5.0 mm maxDrive screws; KLS Martin, Tuttlingen, Germany) on the maxilla for bone-anchored fiducial registration, and 14 polyetheretherketone (PEEK) Allen screws to serve as target positions at the following anatomical landmarks: orbital rim (bilaterally), zygomatic prominence (bilaterally), lateral orbital wall (bilaterally), porion (bilaterally), nasion, frontal bone (bilaterally), cranium, and occipital bone (bilaterally). A computed tomography (CT) scan was acquired and imported into the Origin/Brainlab environment (iPlan version 3.0.6; Brainlab AG, Munich, Germany). A virtual landmark was indicated on the Allen screw positions. The coordinates of these landmarks were used as the ground truth in the target registration error (TRE) quantification.[2,13,14] The experimental setup is visualized in *Figure 1*.

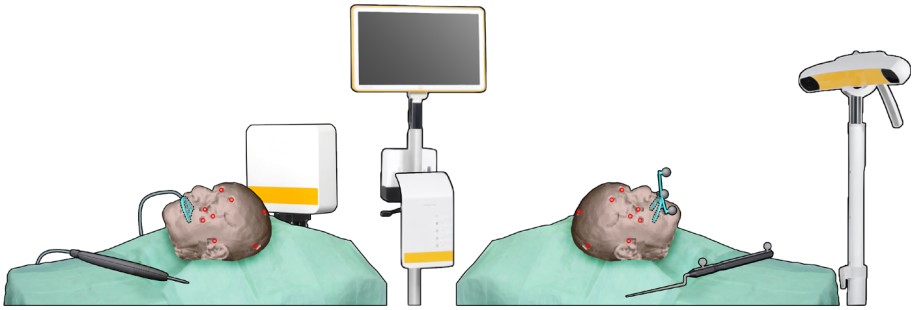

Figure 1. Schematic overview of the experimental setup. *The electromagnetic tracking setup is shown on the left side, with the field generator positioned lateral to the cadaver head. The DRF is positioned in the holder on the splint (detailed design in Figure 2f). On the right, the optical setup with the splint-attached DRF in place is visualized. The red circles indicate the positions of the Allen target screws.*

Conventional methods

TRE assessment

The Kick navigation system (Brainlab AG, Munich, Germany) was used for all measurements since this system is compatible with optical and EM tracking. Brainlab's craniomaxillofacial module (CMF) was used for optical navigation; soft-tissue registration was not available in this module. The ENT module was used for all EM measurements. The DRF corresponding to the tracking method was attached to the lateral skull. Bone-anchored fiducial registration was performed by indicating the five inserted maxillary screws; the virtual registration points had been indicated in the Brainlab environment. Each observer (RS, FB) performed five repetitions of registration with bone-anchored fiducials with optical tracking and five repetitions of bone-anchored fiducial registration with EM tracking. Soft-tissue registration with EM tracking was performed according to the instructions provided by the system. This registration was repeated five times by both observers as well. After each registration, the navigation instrument was positioned at the Allen screws (target positions), and the coordinates were stored through the 'Acquire' functionality.

Experimental method

Theoretical background

Mathematically, the registration procedure determines the transformation of the DRF from its reference position to the position in the patient image volume. In other terms, $\mathbf{T}_{reg}$, the transformation obtained through the registration procedure, provides an approximation of $\mathbf{T}_{DRF}$, the actual position of the DRF in the image volume. After registration is completed, $\mathbf{T}_{reg}$ is stored by the navigation system. The navigation system also expresses the position of any pointer as a transformation matrix describing the position and orientation within the patient: $\mathbf{T}_{PTR}$. In practice, $\mathbf{T}_{PTR}$ is calculated by the navigation system from $\mathbf{T}_{reg}$ and the difference in tracking position between the DRF and the pointer ($\mathbf{T}_{DRF \rightarrow PTR}$). In TRE measurements, the position of the pointer's tip (translation component $\mathbf{t}_{PTR}$ of $\mathbf{T}_{PTR}$) is compared to the virtual landmark position. An overview of the transformations involved in the process and their underlying connections is provided in Appendix I; a schematic drawing of the registration-free approach is shown in Appendix I *Figure I*. The hypothesis behind the registration-free approach is that the DRF may be inserted at a known position in the image volume and $\mathbf{T}_{DRF}$ could be determined/approximated preoperatively, rendering any intraoperative registration mute.

Practical implementation

The maxillary dentition was identified as a suitable anatomical structure to attach the DRF in a known and stable position. An intraoral scan of the maxillary dentition (TRIOS 3 intraoral scanner; 3Shape, Copenhagen, Denmark) was acquired to obtain a detailed virtual stereolithographic model (STL) of the dentition. The CT scan was imported in IPS CaseDesigner (version 1.4; KLS Martin, Tuttlingen, Germany), and the maxillary dental model was fused to the maxillary dentition of the CT scan.[15] The fused dental model was exported from IPS as an STL. In Blender (version 2.81; Blender Foundation, Amsterdam, The Netherlands), the maxillary dental model was imported, and a splint fitting the dentition was designed. An offset of 0.1 mm for the dental model was used to ensure proper splint fit. Two augmentations of the splint were implemented to equip it with DRFs: one to equip the splint with reflective markers resembling the Skull Reference Array (Brainlab AG, Munich, Germany) for optical navigation and one resembling the EM Reference Holder (Brainlab AG, Munich, Germany). The design of the splint took approximately 15–20 minutes. An outline of the registration-free workflow and a visualization of the designs are provided in *Figure 2*. The designs were exported as STLs and manufactured through 3D printing with a PolyJet printer (Objet30 Prime; Stratasys Ltd., Eden Prairie, MN, USA). The designs were manufactured in a transparent material (VeroClear). Brainlab provided the geometries, configurations, and reference positions of the optical and EM DRF.

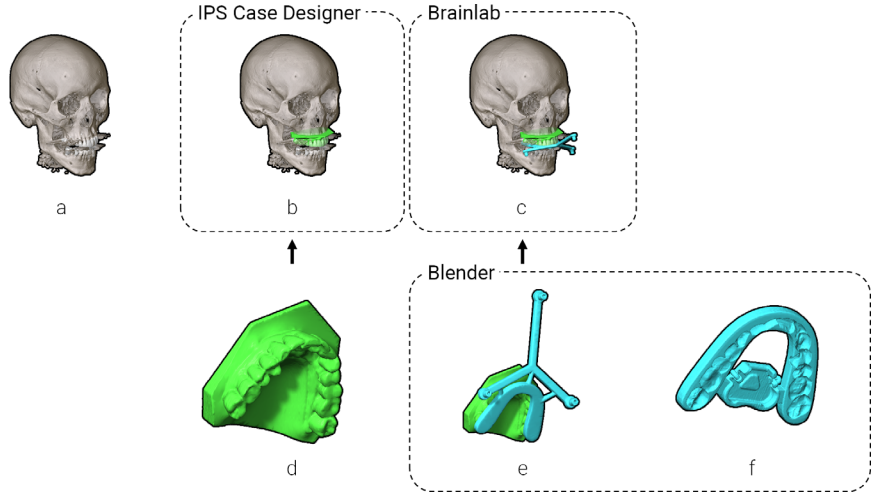

Figure 2. Workup of the registration-free workflow and the software used. *Steps a, b, and d are identical to the steps in* **Chapter 9***: The CT scan (a) and intraoral scan (d) are fused in IPS Case Designer (b). A splint-borne DRF is designed for optical tracking (e), and a splint-borne DRF holder is designed for EM tracking (f). After transformation, the DRF may be visualized in the Brainlab environment (c), and the position of the DRF may be used as .*

The splint-borne DRF meets the prerequisite of a preoperatively established position of the DRF in the image volume. The transformation of the DRF to the position on the splint (in the IPS CaseDesigner patient model, $\mathbf{T}_{SPL(IPS)}$) was calculated in Blender. IPS CaseDesigner and Brainlab software construct their reference frames differently (voxel space and image space) and use a different image orientation (RAS and LPS). As a consequence, an additional transformation is necessary to obtain the position of the splint-borne DRF in the Brainlab coordinate system ($\mathbf{T}_{SPL(BL)}$). The necessary information to obtain $\mathbf{T}_{IPS \rightarrow BL}$ was extracted from the ImagePositionPatient (IPP) information in the DICOM header file of the CT scan (Appendix I).

When the splint-borne DRF is positioned during surgery, $\mathbf{T}_{SPL(BL)}$ provides a preoperative approximation of the DRF's position in the patient image volume and can thus be used as a substitute for the intraoperatively defined $\mathbf{T}_{reg}$: the need for intraoperative registration would be obsolete.

TRE assessment

Currently, the navigation software is not equipped with the functionality to set $\mathbf{T}_{DRF}$ preoperatively: a registration procedure is mandatory to use the navigation hardware. A temporary preregistration procedure was performed ($\mathbf{T}_{reg}$) solely as a workaround to meet the system's demands. $\mathbf{T}_{SPL(BL)}$ is introduced as a substitute approximation of $\mathbf{T}_{DRF}$ afterward. In the EM measurements, the DRF was positioned on the splint, and the preregistration was performed using surface-based registration. In the optical navigation setting, the preregistration was performed while the Skull Reference Array was fixated to the cadaver's skull; point-based fiducial registration was used to determine $\mathbf{T}_{reg}$. The Skull Reference Array was subsequently removed and replaced by the splint-borne DRF. In both tracking techniques, the splint was secured using power chains. The landmark positions $\boldsymbol{c}$ were obtained similar to bone-anchored fiducial registration and surface-based registration: five repetitions were performed by each observer (RS, FB) for each tracking technique (optical, EM). The splint was repositioned after each repetition since this is the primary act that determines the measurement outcome.

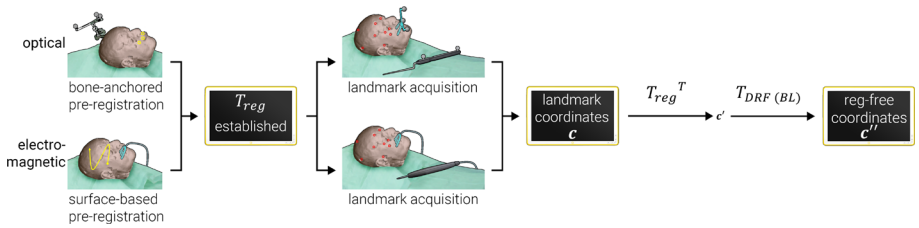

Figure 3. Flow chart of the transformations in the registration-free workflow. *Two different overviews are presented: the method utilized in optical tracking is seen above, and the method in electromagnetic tracking is visualized below.*

A recalculation of the data was performed (Appendix I) to assess the TRE in registration-free navigation. First, the coordinate positions were transformed by $\mathbf{T}_{reg}{}^{T}$ to correct the preregistration. The transformation yields an expression of the measured landmarks relative to the DRF: $\boldsymbol{c'}$. Subsequently, the landmark coordinates were transformed by $\mathbf{T}_{SPL(BL)}$ to obtain their image coordinate in the registration-free navigation workflow ($\boldsymbol{c''}$). A flow chart is presented in *Figure 3*, which documents the different transformations in the registration-free measurement process.

Data processing

The data for each measurement session were stored in DICOM format and exported from the navigation system. In Matlab (version 2019b; the MathWorks Inc., Natick, MA, USA), the acquired landmarks were extracted from the DICOM data. Recalculation of the registration-free coordinates (as described in the subsection above) was performed in Matlab as well. The Euclidean distance between the resulting coordinates and the target coordinates was calculated (TRE); the Euclidean distances were exported as comma-separated values. A linear mixed model incorporating all measurements was generated in R.[16,17] The fixed effects were tracking technique, registration method, target distance, and their interactions. The target distance was calculated as the distance of a fiducial to the centroid of the splint. The mean target distance of the infraorbital rim landmarks was calculated and subtracted from all target distances. This ensured that a clinically meaningful intercept was provided: the linear-mixed-model outcome at distance = 0 represents the accuracy at the infraorbital rim.

Results

TABLE 1. Fixed-effect estimates. Bone-anchored registration with optical tracking was the model's reference category. The bold font indicates the registration-free parameters.

Fixed effect	Estimate	sd	t-value
(Intercept)	0.970	0.0348	27.86
Distance	+0.005	0.0002	23.07
EM technique	−0.064	0.0202	−3.19
Registration-free	**+0.188**	**0.0202**	**9.31**
Surface-based registration	+0.197	0.0202	9.78
Distance:EM technique	−0.001	0.0003	−2.35
Distance:Registration-free	**−0.001**	0.0003	**−3.13**
Distance:Surface-based registration	−0.003	0.0003	−9.73
EM technique:Registration-free	**−0.253**	**0.0286**	**−8.87**
Distance:EM technique:Registration-free	**+0.000**	**0.0004**	**0.86**

1396 measurements were obtained using registration-free navigation, 4 (0.3%) were missing (1 registration method x 2 tracking systems x 2 observers x 5 repetitions x 5 cadavers x 14 target points – 4). In total, 3496 data points were included in the results (1396 registration-free (2 tracking methods), 1400 bone-anchored fiducials (2 tracking methods), and 700 soft-tissue registration (EM tracking)). Histograms and kernel density estimates for TRE and $\sqrt{\text{TRE}}$ are provided for registration-free navigation in *Figure 4* and histograms and kernel density estimates for bone-anchored fiducials and soft-tissue registration in **Chapter 9** (*Figure 3* and *4*). The $\sqrt{\text{TRE}}$ data distributions most closely represent a normal distribution. In Table 1, the fixed-effect estimates of the complete linear mixed model are provided. The data are recalculated to an intercept value (at the infraorbital rim's level) and a slope value (the increase of $\sqrt{\text{TRE}}$ per mm distance from the intercept) for each combination of registration method and tracking technique in Table 3. In *Figure 5*, $\sqrt{\text{TRE}}$ is plotted against target distance for all combinations, using the acquired slope and intercept values.

TABLE 2. Intercept and slope values from linear-mixed-model parameters.

Tracking	Registration	Intercept	Slope
Optical	Bone-anchored fiducials	0.97	0.0049
Optical	**Registration-free**	**1.16**	**0.0039**
Electromagnetic	Bone-anchored fiducials	0.91	0.0042
Electromagnetic	**Registration-free**	**0.84**	**0.0036**
Electromagnetic	Surface-based	1.10	0.0013

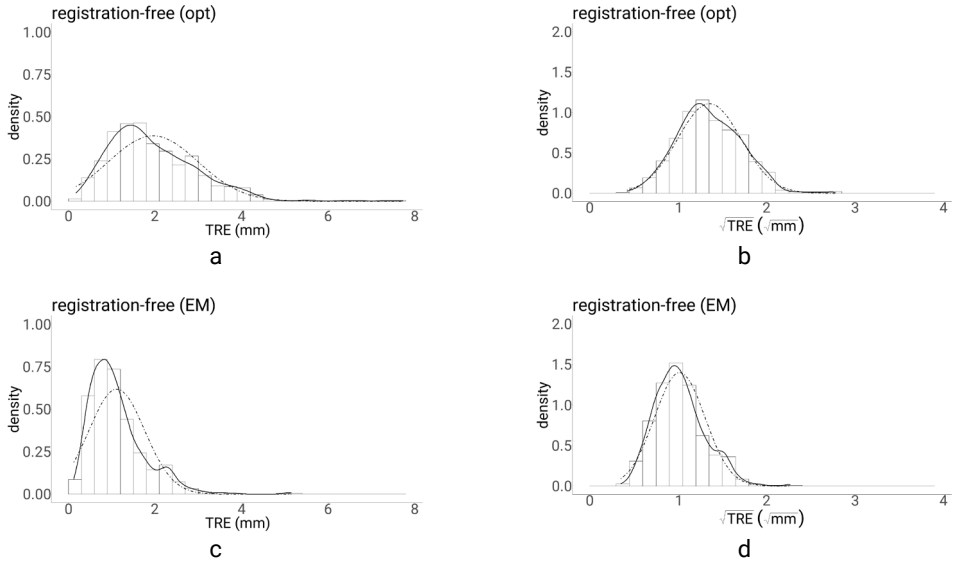

Figure 4. Distribution of TRE (a and c) and $\sqrt{TRE}$ (b and d) for the registration-free navigation approach. *The dashed line represents a normal distribution with the mean and standard deviation of the outcome measure. From these histograms, it is seen that the $\sqrt{TRE}$ distribution has a better resemblance to the normal distribution.*

The plot in *Figure 5* demonstrates that the EM registration-free approach outperforms all other registration approaches, but the optical registration-free approach is outperformed by bone-anchored fiducial optical registration and all EM registration approaches. In *Figure 6*, combined kernel-density-estimate and scatter plots are given for the registration-free data. The regression lines from *Figure 5* are superimposed on the scatter plots. For the EM registration-free measurements, 11% of TRE measurements was > 2mm; for the optical measurements, this was 41% (compared to 27% for optical bone-anchored fiducials, 15% for EM bone-anchored fiducials, and 17% for EM soft-tissue registration).

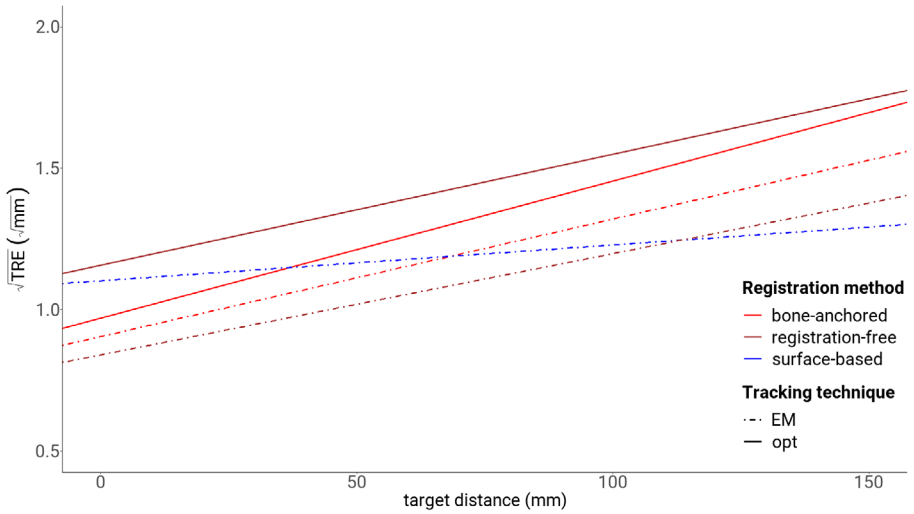

Figure 5. Visualization of the regression lines for each registration method and tracking technique. *The brown lines show the registration-free technique.*

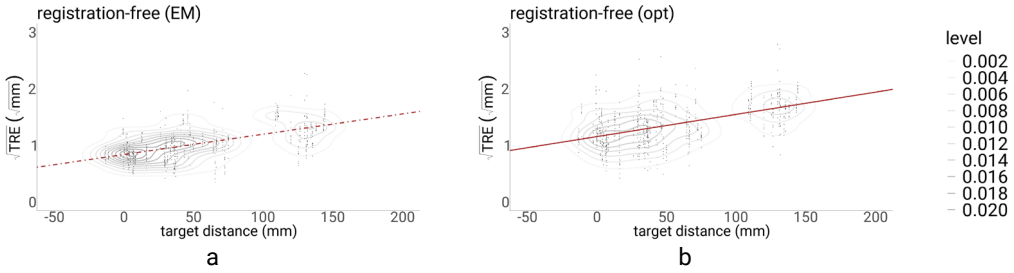

Figure 6. Scatter plots, with kernel-density-estimate levels for the registration-free workflow in electromagnetic (a) and optical (b) tracking. *The regression lines from Figure 5 are superimposed. The EM measurements are less scattered than the optical measurements.*

Discussion

A novel registration-free approach for craniofacial surgical navigation was introduced in this study. The target accuracy of the method was evaluated and compared to the accuracy of bone-anchored fiducial registration and surface-based registration. Bone-anchored fiducial registration proved more accurate at the infraorbital rim but was more heavily affected by increasing target distance than soft-tissue registration. The increased accuracy at the infraorbital rim may be explained by the proximity of this landmark to the registration fiducials. The limited variation in the craniocaudal direction of the fiducials gives rise to a relative coplanar orientation, which is known to yield increasing TRE values moving away from the registration centroid.[18] The configuration of the bone-anchored fiducials was chosen to mimic the clinical setting as closely as possible rather than aim for the optimal TRE value. The registration-free approach yielded excellent results compared to conventional approaches with EM tracking, but the results of the optical tracking setting were unfavorable to any of the alternative intraoperative registration methods. This significant deviation between the tracking methods makes

the results difficult to interpret. The deviating results between both tracking techniques are unexpected. Two differences can be distinguished between the registration-free procedure for EM and optical navigation: one regarding design and one regarding preregistration procedure. These differences and their possible effect on registration accuracy are detailed below, but neither provides a solid explanation for the difference or its magnitude.

The attachment of the DRF on the registration splint is different between optical and EM tracking. The EM tracker is positioned within a holder on the splint; the holder attaches to the splint's molar region on both sides. The optical tracker is not attached to the design but is incorporated in it: the reflective markers are attached to three arms extending on the mesial side of the central incisors. While direct incorporation in the design should be less error-prone, the optical design may suffer from reduced stiffness in the material because of the extensions' length, which might have affected the actual position of the reflective marker spheres and the complete DRF. Venosta et al. noticed the influence of material stiffness on registration accuracy in their extended splint design.[5] The DRF splint was designed bearing maximum bending resistance in mind: a rounded edge design was chosen for the extensions over a cubic one for precisely this reason. The location of the DRF in relation to the dentition might also have influenced positioning accuracy. After securing the splint, position deviation of the DRF in EM may be primarily due to differences in splint fit on the molars, while a positional deviation of the optical tracker may occur because of a difference in fit between the molar region and the incisors. Ye et al. have investigated splint fit, and, in their results, a difference in splint fit between the incisor region and the molars can be seen.[19] However, this difference is only minimal, and the recommended offset of 0.1 mm, which resulted in the smallest fit deviation, was used in this study.

The second difference was in the mandatory preregistration (performed to meet the requirements of the navigation system but corrected by the back-transformation). As stated in the methods section, the EM DRF was positioned on the splint during preregistration (with surface-based matching), while the optical skull-fixated optical DRF was exchanged for the splint-borne DRF. This workflow was chosen because surface-based matching was not available in the optical setting, and the position of the splint-borne DRF would interfere with the registration process on the bone-anchored fiducials. The landmarks collected with the 'Acquire' functionality were outside the image volume assigned in the DICOM information in the optical tracking, but their coordinates were still registered. The preregistration transformation and any error associated with it were corrected similarly for optical and EM tracking, so this should not have influenced the registration-free TRE measurements. The orientation difference between the skull-fixated and splint-borne DRFs might give rise to some technical error in measuring the positions of the reflective marker spheres by the optical camera, but this error is not expected to be in the order of magnitude of the TRE difference. A final explanation might be an inaccuracy in the design or fabrication of the optical splint-borne DRF. The virtual designs were checked, and the geometry of the reflective marker spheres was controlled with distance measurements. No substantial errors were found using these methods, and the navigation system recognized all splint-borne DRFs; any significant deviation in design or manufacturing would have precluded recognition.

Several studies have proposed designs of a DRF supported by a splint.[20–31] This position of the DRF may be less invasive than fixation to the patient's cranium.[32] Registration outside the patient has been proposed, both with a fiducial-based [20,21,26,27,29–31] and automatic method.[22,23,25,28] The fiducial-based registration is possible if the design has registration fiducials and the DRF attached to the splint. The splint and the fiducials need to be positioned in the patient's mouth during scan acquisition; the DRF may be rigidly fixated to the splint or attached later. The relationship between the fiducials and the DRF will not change, so registration can be performed before the splint is positioned in the patient's mouth. A prerequisite is that the splint position does not differ between image acquisition and surgical setting. This workflow is still susceptible to fiducial localization errors in the image volume and physical space

since a registration still needs to be performed.[4] In the automatic registration methods proposed, the DRF is connected to the splint and present in the image volume, or a unique connection between splint and DRF is designed. The position of the DRF in the image volume, and thus $\mathbf{T}_{reg}$, may be determined on the preoperative scan. This method is similar to the registration process described here but requires image acquisition with the splint in position, which frequently leads to acquisition of a second scan and additional radiation exposure for the patient.

Intraoperative automatic image registration suffers from the same drawback. In this workflow, the DRF is fixated intraoperatively and tracked with the optical camera during cone-beam CT acquisition.[7,10,12,33] This method yields an accurate registration, even if low-dose scan protocols are used, but may lead to an increase in operation time and pose logistical challenges intraoperatively.[10,12] A compatible intraoperative scanner is required, and, currently, this method is only available for optical tracking. Other methods of user-independent registration have been proposed: a stereotactic mask, which uses active LEDs, or three-dimensional (3D) stereophotogrammetry to capture the soft tissue of the patient with the DRF in place.[9,34–36] The stereotactic mask is attached to the patient's face and used for both registration and tracking, which means that the mask has to stay attached during the complete procedure. This requirement may limit its application in reconstructive surgery of the midface.[9,35] With 3D stereophotogrammetry, the soft-tissue surface is captured through photographs of the patient with the DRF in place.[34–36] A large surface of the skin needs to be exposed for the photographs, and methods relying on soft tissue are susceptible to skin surface alterations. Thus, these methods may not be applicable when soft-tissue variation is expected (e.g., swelling or nasal intubation).[9,36]

The dentition may be used as a reference directly or indirectly in augmented reality (AR).[37–39] Wang et al. designed a method in which an intraoral scan is matched to the CT scan (based on an iterative closest point approach).[39] The visible teeth of the patient are tracked with a stereo camera. After registering the stereo camera images with the intraoral scan model, the physical world can be augmented with the VSP. Exposure of the dentition within the field of view is a requirement for the workflow. Jiang et al. have proposed an AR workflow resembling the registration-free workflow described in this study.[37] An intraoral scan of the gypsum cast with the DRF in place is acquired, and the resulting model is matched to the CT scan using user-indicated landmarks on the dental cusps in the CT model and intraoral scan. In the workflow described in the current study, the DRF is not positioned during the intraoral scan, which allows an intraoral scan of the complete dentition. Moreover, the algorithm that matches the dental model on the CT scan is not user-dependent. These differences in approach may improve the matching accuracy of the intraoral scan for the current method but might lack control of the splint fit on the dentition.[40]

The registration-free navigation workflow is a method that is noninvasive and not user-dependent. It is compatible with both optical and EM navigation. It could lead to a more time-efficient intraoperative procedure since intraoperative registration is obviated. Clinical implementation would require embedding the workflow in a commercial navigation system so that the registration matrix is determined directly rather than correcting the preregistration as done in this study. The workflow may be used in (partly) dentate patients whose maxillary complex is intact and continuous with the cranium. Fixation of the splint without affecting the noninvasive character of the method should be improved. Ideally, the splint would snap in place on the dentition. The method proved accurate if EM tracking was used. In contrast, a significant error was found if optical tracking was used. No clear explanation for the difference between optical and EM navigation was found, although the accuracy in the optical navigation setting might improve to some extent if material stiffness and splint design are optimized. The biggest challenge toward implementing the workflow lies in reducing the error in optical navigation.

Conclusion

A registration-free workflow for optical and EM craniofacial surgical navigation was presented in this study. This method offers a noninvasive, user-independent alternative to existing registration procedures and may increase time efficiency intraoperatively. The method's accuracy was evaluated on five human cadaver heads; the results were compared to accuracy measurements of maxillary bone-anchored fiducials (optical and EM) and surface-based registration (EM). The registration-free accuracy for optical and EM tracking differs significantly. The results for EM tracking are auspicious, while registration-free optical navigation was the least accurate of all methods. Although the workflow itself is promising, this difference in results without a valid explanation hampers direct clinical implementation.

ACKNOWLEDGMENTS

We would like to thank N.H.J. Lobé (Department of Radiology) for the design of the imaging protocol and the acquisition of the CT scans. We would like to thank M. Clerckx from the Department of Medical Biology, Section Clinical Anatomy and Embryology for the support in the cadaver lab. We are grateful for the 3D printing of the splints by C. Kes, M. Rijpkema, and M.M. Steenmetz (tool shop Amsterdam University Medical Centers, location AMC). M.D.J. Wolvers from the Clinical Research Unit was consulted for the statistical analysis. Finally, we are thankful for the in-kind support by Brainlab AG (Kick navigation system, navigation instruments) and KLS Martin (titanium screws).

REFERENCES

1. Widmann G., Stoffner R., Bale R. Errors and error management in image-guided craniomaxillofacial surgery. *Oral Surgery, Oral Med Oral Pathol Oral Radiol Endodontology* 2009;**107**(5):701–15.
2. Eggers G., Mühling J., Marmulla R. Image-to-patient registration techniques in head surgery. *Int J Oral Maxillofac Surg* 2006;**35**(12):1081–95.
3. Luebbers H-T., Messmer P., Obwegeser JA., Zwahlen RA., Kikinis R., Graetz KW., et al. Comparison of different registration methods for surgical navigation in cranio-maxillofacial surgery. *J Cranio-Maxillofacial Surg* 2008;**36**(2):109–16.
4. Fitzpatrick JM. The role of registration in accurate surgical guidance. *Proc Inst Mech Eng Part H J Eng Med* 2010;**224**(5):607–22.
5. Venosta D., Sun Y., Matthews F., Kruse AL., Lanzer M., Gander T., et al. Evaluation of two dental registration-splint techniques for surgical navigation in cranio-maxillofacial surgery. *J Cranio-Maxillofacial Surg* 2014;**42**(5):448–53.
6. Boeckx P., Essig H., Kokemuller H., Tavassol F., Gellrich NC., Swennen GRJ. Presentation and evaluation of a modified wax-bite dental splint for surgical navigation in craniomaxillofacial surgery. *J Oral Maxillofac Surg* 2015;**73**(11):2189–95.
7. Grauvogel TD., Becker C., Hassepass F., Arndt S., Laszig R., Maier W. Comparison of 3D C-Arm–Based Registration to Conventional Pair-Point Registration Regarding Navigation Accuracy in ENT Surgery. *Otolaryngol Neck Surg* 2015;**152**(2):266–71.
8. Ballesteros-Zebadúa P., García-Garduño OA., Galván de la Cruz OO., Arellano-Reynoso A., Lárraga-Gutiérrez JM., Celis MA. Assessment of an image-guided neurosurgery system using a head phantom. *Br J Neurosurg* 2016;**30**(6):606–10.
9. Grauvogel TD., Engelskirchen P., Semper-Hogg W., Grauvogel J., Laszig R. Navigation accuracy after automatic-and hybrid-surface registration in sinus and skull base surgery. *PLoS One* 2017;**12**(7):e0180975.
10. Carl B., Bopp M., Saß B., Pojskic M., Gjorgjevski M., Voellger B., et al. Reliable navigation registration in cranial and spine surgery based on intraoperative computed tomography. *Neurosurg Focus* 2019;**47**(6):E11.
11. Yu H., Shen SG., Wang X., Zhang L., Zhang S. The indication and application of computer-assisted navigation in oral and maxillofacial surgery—Shanghai's experience based on 104 cases. *J Cranio-Maxillofacial Surg* 2013;**41**(8):770–4.
12. Carl B., Bopp M., Saß B., Nimsky C. Intraoperative computed tomography as reliable navigation registration device in 200 cranial procedures. *Acta Neurochir (Wien)* 2018;**160**(9):1681–9.
13. Maurer CR., Fitzpatrick JM., Wang MY., Galloway RL., Maciunas RJ., Allen GS. Registration of head volume images using implantable fiducial markers. *IEEE Trans Med Imaging* 1997;**16**(4):447–62.
14. Fitzpatrick JM., West JB. The distribution of target registration error in rigid-body point-based registration. *IEEE Trans Med Imaging* 2001;**20**(9):917–27.
15. Swennen GRJ., Gaboury M. Imaging Workflow for 3D Virtual Treatment Planning of Orthognathic Surgery. *3D Virtual Treatment Planning of Orthognathic Surgery*. Springer; 2017. p. 1–52.
16. Team RC. R: A language and environment for statistical computing 2019.
17. Bates D., Mächler M., Bolker B., Walker S. Fitting linear mixed-effects models using lme4. *J Stat Softw* 2015;**67**(1):1–48.
18. Fitzpatrick JM., West JB., Maurer CR. Predicting error in rigid-body point-based registration. *IEEE Trans Med Imaging* 1998;**17**(5):694–702.

19. Ye N., Wu T., Dong T., Yuan L., Fang B., Xia L. Precision of 3D-printed splints with different dental model offsets. *Am J Orthod Dentofac Orthop* 2019;**155**(5):733–8.

20. Bale RJ., Burtscher J., Eisner W., Obwegeser AA., Rieger M., Sweeney RA., et al. Computer-assisted neurosurgery by using a noninvasive vacuum-affixed dental cast that acts as a reference base: another step toward a unified approach in the treatment of brain tumors. *J Neurosurg* 2000;**93**(2):208–13.

21. Ledderose GJ., Hagedorn H., Spiegl K., Leunig A., Stelter K. Image guided surgery of the lateral skull base: testing a new dental splint registration device. *Comput Aided Surg* 2012;**17**(1):13–20.

22. Lin L., Gao Y., Chai G., Xu H., Xie L. Electromagnetic Navigation in Craniofacial Surgery Based on Automatic Registration of Dental Splints. *J Craniofac Surg* 2020;**31**(2):393–6.

23. Aydemir CA., Arısan V. Accuracy of dental implant placement via dynamic navigation or the freehand method: A split-mouth randomized controlled clinical trial. *Clin Oral Implants Res* 2020;**31**(3):255–63.

24. Cho B., Oka M., Matsumoto N., Ouchida R., Hong J., Hashizume M. Warning navigation system using real-time safe region monitoring for otologic surgery. *Int J Comput Assist Radiol Surg* 2013;**8**(3):395–405.

25. Li B., Zhang L., Sun H., Shen SGF., Wang X. A new method of surgical navigation for orthognathic surgery: optical tracking guided free-hand repositioning of the maxillomandibular complex. *J Craniofac Surg* 2014;**25**(2):406–11.

26. Zhang W., Wang X., Zhang J., Shen G. Application of preoperative registration and automatic tracking technique for image-guided maxillofacial surgery. *Comput Assist Surg* 2016;**21**(1):137–42.

27. Naujokat H., Rohnen M., Lichtenstein J., Birkenfeld F., Gerle M., Flörke C., et al. Computer-assisted orthognathic surgery: evaluation of mandible registration accuracy and report of the first clinical cases of navigated sagittal split ramus osteotomy. *Int J Oral Maxillofac Surg* 2017;**46**(10):1291–7.

28. Panchal N., Mahmood L., Retana A., Emery R. Dynamic Navigation for Dental Implant Surgery. *Oral Maxillofac Surg Clin* 2019;**31**(4):539–47.

29. Ma L., Jiang W., Zhang B., Qu X., Ning G., Zhang X., et al. Augmented reality surgical navigation with accurate CBCT-patient registration for dental implant placement. *Med Biol Eng Comput* 2019;**57**(1):47–57.

30. Sukegawa S., Yoneda S., Kanno T., Tohmori H., Furuki Y. Optical surgical navigation-assisted removal of a foreign body using a splint to simplify the registration process: a case report. *J Med Case Rep* 2019;**13**(1):209.

31. Yamamoto S., Taniike N., Takenobu T. Application of an open position splint integrated with a reference frame and registration markers for mandibular navigation surgery. *Int J Oral Maxillofac Surg* 2020;**49**(5):686–90.

32. Iwai T., Mikami T., Yasumura K., Tohnai I., Maegawa J. Use of occlusal splint for noninvasive fixation of a reference frame in orbital navigation surgery. *J Maxillofac Oral Surg* 2016;**15**(3):410–2.

33. Zhao J., Liu Y., Fan M., Liu B., He D., Tian W. Comparison of the clinical accuracy between point-to-point registration and auto-registration using an active infrared navigation system. *Spine (Phila Pa 1976)* 2018;**43**(22):E1329–33.

34. Fan Y., Yao X., Hu T., Xu X. An Automatic Spatial Registration Method for Image-Guided Neurosurgery System. *J Craniofac Surg* 2019;**30**(4):e344–50.

35. Wu CY., Kahana A. Stereotactic navigation with a registration mask in orbital decompression surgery: preliminary results. *Ophthal Plast Reconstr Surg* 2015;**31**(6):440–4.

36. Fan Y., Jiang D., Wang M., Song Z. A new markerless patient-to-image registration method using a portable 3D scanner. *Med Phys* 2014;**41**(10):101910.

37. Jiang T., Zhu M., Chai G., Li Q. Precision of a novel craniofacial surgical navigation system based on augmented reality using an occlusal splint as a registration strategy. *Sci Rep* 2019;**9**(1):1–8.

38. Wang J., Suenaga H., Yang L., Kobayashi E., Sakuma I. Video see-through augmented reality for oral and maxillofacial surgery. *Int J Med Robot Comput Assist Surg* 2017;**13**(2):e1754.

39. Wang J., Shen Y., Yang S. A practical marker-less image registration method for augmented reality oral and maxillofacial surgery. *Int J Comput Assist Radiol Surg* 2019;**14**(5):763–73.

40. Baan F., Bruggink R., Nijsink J., Maal TJJ., Ongkosuwito EM. Fusion of intra-oral scans in cone-beam computed tomography scans. *Clin Oral Investig* 2021;**25**(1):77–85.

APPENDIX I

Overview of transformations and coordinates

Theoretical background

$\mathbf{T}_{DRF}$: transformation of Dynamic Reference Frame from its reference position to the position in the patient image volume. Represents the actual position of the reference frame in the image volume.

$\mathbf{T}_{reg}$: approximation of $\mathbf{T}_{DRF}$, obtained through an intra-operative registration procedure. $\mathbf{T}_{reg}$ can be extracted from the DICOM header information stored in the navigation system. Represents the approximated position of the reference frame in the image volume.

$\mathbf{T}_{PTR}$: position of the navigation pointer instrument in the image volume. In practice, the coordinates of the pointer's tip ($\mathbf{t}_{PTR}$) are stored in the TRE measurements, using the 'Acquire'-functionality.

$\mathbf{T}_{DRF \rightarrow PTR}$: transformation between DRF position and pointer position, used in practice to calculate $\mathbf{T}_{PTR}$ by the navigation system.

Practical implementation

$\mathbf{T}_{SPL(IPS)}$: transformation of the DRF from its reference position to the position on the splint (in the IPS coordinate system). This transformation can be extracted (preoperatively) from the splint design in the Blender environment.

$\mathbf{T}_{IPS \rightarrow BL}$: transformation used to transform objects (in this case, the spint-borne DRF) from the IPS coordinate system to the Brainlab coordinate system. The information to construct this transformation is extracted from the DICOM header tag (0020,0032) (ImagePositionPatient, IPP) of the preoperative CT scan:

$$\mathbf{T}_{IPS \rightarrow BL} = \begin{bmatrix} -1 & 0 & 0 & -X_{IPP} \\ 0 & -1 & 0 & -Y_{IPP} \\ 0 & 0 & 1 & Z_{IPP} \\ 0 & 0 & 0 & 1 \end{bmatrix}$$

$\mathbf{T}_{SPL(BL)}$: transformation from the DRF's reference position to its position in the Brainlab coordinate system. This transformation is used as a pre-operatively defined approximation of $\mathbf{T}_{DRF}$ in the registration-free workflow.

Registration-free TRE measurement

$\boldsymbol{l}$: coordinates of the landmark in the image volume.

$\boldsymbol{c}$: coordinates of $\boldsymbol{l}$ as acquired by the navigation system.

$\boldsymbol{c'}$: coordinates of $\boldsymbol{c}$, corrected for pre-registration.

$\boldsymbol{c''}$: measured coordinates of $\boldsymbol{l}$ in the registration-free workflow.

N.B. bold notation indicates a vector of all landmark coordinates.

Schematic drawings

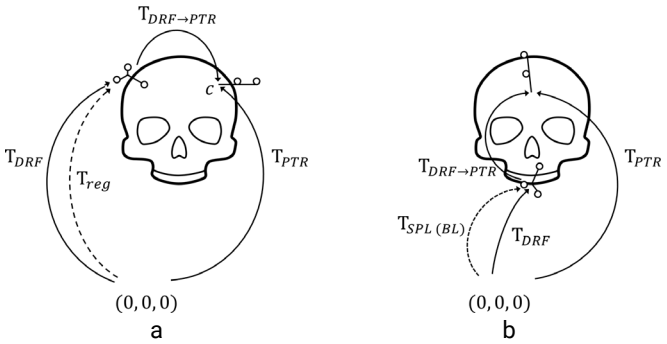

Appendix I Figure I. Theoretical background of registration-free navigation. *In a normal registration procedure (a), the actual position of the DRF (*$\mathbf{T}_{DRF}$*) isapproximated by a registration procedure, resulting in (*$\mathbf{T}_{reg}$*). The pointer position is expressed as* $\mathbf{T}_{PTR}$ *in the image volume; in practice, this position is calculated from the transformation between DRF and pointer (*$\mathbf{T}_{DRF \rightarrow PTR}$*). In the registration-free approach, the DRF is positioned on a splint. The planned position of the DRF in the image volume (*$\mathbf{T}_{SPL(BL)}$*) is known pre-operatively and is used as an approximation of* $\mathbf{T}_{DRF}$*, rendering intra-operative registration mute.*

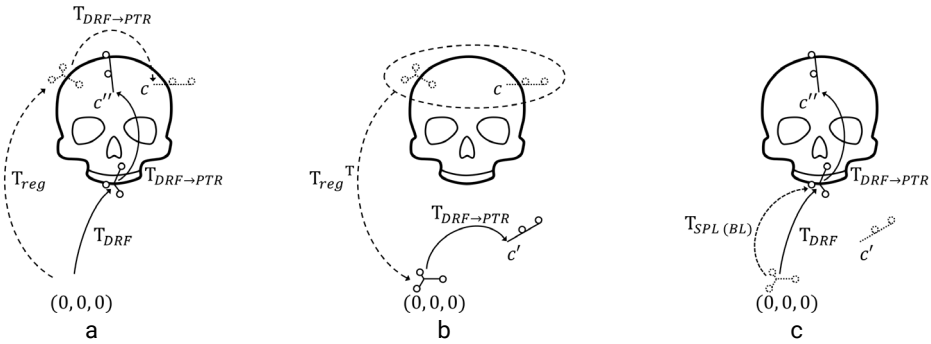

Appendix I Figure II. Registration-free TRE measurement. *This is a workaround, since it is not feasible to set* $\mathbf{T}_{SPL(BL)}$ *as the approximation of* $\mathbf{T}_{DRF}$*. A pre-registration (corrected later on) is performed with the reference frame attached to the lateral skull (*$\mathbf{T}_{reg}$*). This DRF is exchanged with the splint-borne DRF. During the TRE measurements, the pointer is positioned at landmark* ***l****. The navigation system will acquire the coordinates associated with* ***c****, from* $\mathbf{T}_{reg}$ *and* $\mathbf{T}_{DRF \rightarrow PTR}$*. In b, a transformation with* $\mathbf{T}_{reg}{}^{T}$ *is performed to the acquired coordinates. The approximated DRF's position (through* $\mathbf{T}_{reg}$*) is transformed to its origin;* $\boldsymbol{c'}$ *is solely determined by* $\mathbf{T}_{DRF \rightarrow PTR}$*. In the final stage,* $\boldsymbol{c'}$ *is transformed by* $\mathbf{T}_{SPL(BL)}$*, the pre-operative approximation of the splint-borne DRF's position (*$\mathbf{T}_{DRF}$*), to obtain coordinates* $\boldsymbol{c''}$*. The TRE is calculated from the difference between* $\boldsymbol{l}$ *and* $\boldsymbol{c''}$*.*

Equations

$$\mathbf{T}_{SPL\ (BL)} = \mathbf{T}_{IPS \rightarrow BL}\ \mathbf{T}_{SPL\ (IPS)}$$

$$\boldsymbol{c'} = \mathbf{T}_{reg}{}^{T}\ \boldsymbol{c}$$

$$\boldsymbol{c''} = \mathbf{T}_{SPL\ (BL)}\ \boldsymbol{c'}$$